Materials Advances

ROYAL SOCIETY OF CHEMISTRY

PAPER

View Article Online
View Journal | View Issue

Cite this: *Mater. Adv.*, 2025, 6, 5742

Micelles based on a poly(2-oxazoline) triblock copolymer containing a pure stereoisomer *E* or *Z*-tetraphenylethylene core for theranostic applications†

Stéphane Hoang,[a] Guillaume Pinna,[b] Marie Vandamme,[b] Magali Allain,[c] Catherine Passirani,[a] Patrick Saulnier[a] and Oksana Krupka *[ad]

Poly(2-oxazoline)s (POx) are among the most promising hydrophilic polymers that can act as a replacement for the overly used poly(ethylene glycol)s (PEG). POx are widely studied due to their similar properties to PEG, such as low toxicity, neutrality and stealth properties, when used as a coating for nanoparticles. In this work, micelles based on a POx triblock copolymer containing a *E* or *Z*-tetraphenylethylene (TPE) derivative core were successfully prepared. The physico-chemical properties of both stereochemically pure *E*/*Z*-micelles were compared throughout the study, ranging from their hydrodynamic size, aggregation-induced emission property and colloidal stability. Their ability to host hydrophobic molecules was studied *in vitro* using HeLa cancer cells by encapsulating the hydrophobic fluorophore 1,1′-dioctadecyl-3,3,3′,3′-tetramethylindocarbocyanine perchlorate (DiI) or anticancer drug 6-(7-nitro-2,1,3-benzoxadiazol-4-ylthio)hexanol (NBDHEX). The Förster resonance energy transfer (FRET) pair TPE-DiI displayed an efficient energy transfer process, as demonstrated by the increase in fluorescence, suggesting the effective cellular internalization of the micelles and making them a potential tool for dual imaging applications. The encapsulation and release of the neoplastic drug NBDHEX, known as a potent glutathione *S*-transferase P1-1 inhibitor, highlighted the major differences in the capacity for delivering NBDHEX between the *E*/*Z*-micelles, emphasizing the importance of controlling the configuration of the TPE unit core in theranostic applications.

Received 14th April 2025,
Accepted 25th June 2025

DOI: 10.1039/d5ma00361j

rsc.li/materials-advances

Introduction

Amphiphilic block copolymers constitute hydrophilic and hydrophobic parts that provide self-assembly properties in an aqueous medium to form supramolecular structures, such as vesicles or micelles.[1] Poly(ethylene glycol) (PEG) is the most predominant hydrophilic polymer block due to its biocompatibility, stealth properties, inexpensiveness and ease of access.[2–4] Although PEG's efficiency has long been proven in the development of nanomedicines, its extensive use in other fields (such as cosmetic, food and cleansing agents) over recent decades has led to the emergence of anti-PEG antibodies, even in patients with no prior exposure to PEG.[5,6] Consequently, PEG-based drugs are detected and eliminated more quickly. This reduces the efficacy of the treatment as a result of the accelerated blood clearance (ABC) phenomenon.[7] With the increasing problems related to the overuse of PEG, several hydrophilic polymers were surveyed as potential substitutes. Among them, POx were one of the most promising candidates.[8–11] This family of polymers, synthesized through cationic ring opening polymerization (CROP) of the corresponding monomers, shares properties with PEG, including high cytocompatibility, excellent water solubility, a non-ionic nature, and ease of synthesis from low to high molecular weights with narrow dispersity.[12] While offering the same benefits as PEG, POx provide additional advantages, primarily the potential for versatile functionalization. Indeed, the water solubility can be adjusted, ranging from the highly hydrophilic poly(2-methyl-2-oxazoline) (PMeOx) to completely water insoluble polymers, by increasing the alkyl side chains, such as

[a] *Univ Angers, Inserm, CNRS, MINT, SFR ICAT, F-49000 Angers, France. E-mail: oksana.krupka@univ-angers.fr*
[b] *Plateforme ARN Interférence (PARI), Institut de Radiobiologie Cellulaire et Moléculaire (iRCM), Université Paris-Saclay, CEA, 92260, Fontenay-aux-Roses, France*
[c] *Univ Angers, CNRS, MOLTECH-Anjou, SFR MATRIX, F-49000 Angers, France*
[d] *Taras Shevchenko National University of Kyiv, 60 Volodymyrska str., 01033 Kyiv, Ukraine*

† Electronic supplementary information (ESI) available: Organic synthesis and characterization data, physico-chemical properties study and additional *in vitro* experiments can be found. CCDC 2428365 and 2428366. For ESI and crystallographic data in CIF or other electronic format see DOI: **https://doi.org/10.1039/d5ma00361j**

poly(2-*n*-butyl-2-oxazoline) (P*n*BuOx).[13,14] Thus, POx can be utilized to design diverse amphiphilic block copolymers for the preparation of micelles by combining hydrophobic and hydrophilic POx.[15–17] Another notable feature of POx is their lower critical solution temperature (LCST) behavior, with poly(2-ethyl-2-oxazoline) (PEtOx) and poly(2-isopropyl-2-oxazoline) (PiPrOx) being the most commonly used hydrophilic POx homopolymers owing to their excellent water solubility and LCST values of approximately 60–70 °C and 30–40 °C, respectively.[18] The LCST can be finely tuned by preparing ideal statistical block copolymers with specific ratios, enabled by the similar polymerization rates achieved through microwave-assisted CROP.[19,20] Moreover, POx chemical structures can be accurately engineered through the living polymerization nature of the CROP, offering a wide range of possible pre- and post-functionalizations by carefully selecting the initiating and terminating agents.[21] Recent studies demonstrated that Förster resonance energy transfer (FRET) efficiency in dye-functionalized POx strongly depends on the polymer chain length and fluorophore positioning, enabling applications in temperature sensing and solid-state fluorescence, thus broadening the functional scope of POx-based materials.[22] Therefore, POx are of great interest as polymer platforms in biomedical applications.

Tetraphenylethylene (TPE) is a common luminogen featuring aggregation-induced emission (AIE). TPE is almost nonemissive in the solubilized state and displays a high fluorescence when aggregated, which is caused by the restriction of intramolecular rotation of the four phenyl groups.[23] TPE is particularly interesting in nanomedicine for its ability to emit fluorescence in a confined space, such as within the hydrophobic core of micelles.[24–26] Interestingly, Kim *et al.* demonstrated the ability to thermally activate the AIE property of TPE by a host–guest complex with γ-cyclodextrin *via* the thermoresponsive behavior of poly(2-isopropyl-2-oxazoline).[27] This effect can be exploited to precisely track micelles *in vitro* and *in vivo* to study their accumulation by monitoring the TPE fluorescence signal.[28] Additionally, the combination of TPE as a donor with a specific dye as an acceptor can lead to fluorescence by FRET. As long as the donor–acceptor pair is close to each other (*i.e.*, no more than 10 nm in distance), the FRET signal can be observed. Upon disassembly of the micelles, the dissociation of the pair will occur, which then leads to the loss of the FRET signal.[29] Thus, such system can be exploited to monitor the integrity of micelles in real-time by luminescent behavior. While AIEgen molecules such as TPE benefit from high local concentrations to induce fluorescence by AIE, non-AIEgen molecules face aggregation-caused quenching (ACQ).[30] To achieve this, TPE is typically introduced into the polymer structure using TPE derivatives as initiators,[31,32] monomers,[33] or by post-functionalization.[25,26,34] Amphiphilic block copolymers bearing a TPE moiety tend to have very low critical micellar concentrations (CMC)[35] due to the cumulative effects of AIE from TPE[36,37] and the amphiphilic nature of the copolymer to self-assemble in an aqueous medium.[24,25] A low CMC value is highly desirable to limit micelle disassembly in extremely diluted media such as blood. However, rare reports can be found using bifunctionalized TPE derivatives as initiators.[31,38] TPE derivatives are usually synthesized by a non-stereoselective McMurry coupling reaction, providing a mixture of *E*/*Z* isomers. Considering that the control of stereochemistry plays a key role in medicinal chemistry and life science, *E*/*Z*-TPE derivatives are reported to display different physico-chemical properties.[39] When introduced into an amphiphile as the central unit between two polymer blocks, the *E*/*Z* configurations modify the self-assembly behaviour of the amphiphile, thus leading to different supramolecular structures, as demonstrated by Chen *et al.*[40]

In this work, our aim was to design AIEgen polymeric triblock copolymer micelles featuring a TPE hydrophobic core, synthesized through CROP using stereochemically pure *E* and *Z*-TPE derivatives as initiators. The micelles were systematically characterized and compared in terms of the critical micellar concentration, size, and encapsulation efficiency, showcasing their potential for effective drug delivery of hydrophobic molecules, including anticancer agents and FRET-active compounds. *In vitro* experiments on HeLa cancer cell lines will further assess the biocompatibility and drug delivery efficiency of the micelles, highlighting their promise for advanced theranostic applications.

Results and discussion

Synthesis and characterization of tetraphenylethylene derivatives

The target *E*/*Z*-TPE derivatives (*E*-TPE-2OTs and *Z*-TPE-2OTs) were synthesized in three steps (Scheme 1). Briefly, a McMurry coupling reaction was carried out using commercially available 4-hydroxybenzophenone in the presence of Zn(0) and $TiCl_4$ in refluxing THF, according to a previously reported procedure.[32] Compound **1** was purified by silica gel column chromatography, but the mixture of *Z* and *E* isomers could not be separated

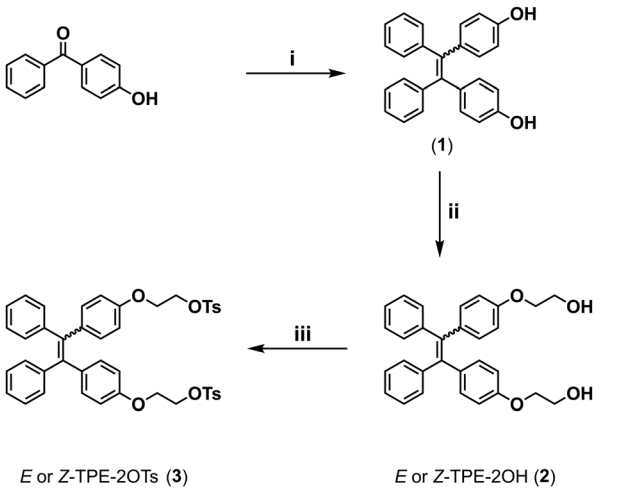

Scheme 1 Synthesis of the initiators *E*/*Z*-TPE-2OTs *via* three steps, (i) Zn, $TiCl_4$, THF, reflux, 36 h; (ii) 2-chloroethanol, KI, K_2CO_3, DMF, 80 °C, 24 h, 53% yield; (iii) TsCl, Et_3N, CH_2Cl_2, rt, 18 h, 28% to 51% yield.

on thin layer chromatography (TLC). The synthesis was pursued by reacting the mixture of isomers with 2-chloroethanol in basic conditions in DMF at 80 °C to yield compound **2**. Remarkably, whereas the two isomers were not separated and used as a mixture in the literature,[32] we successfully separated them by silica gel column chromatography using petroleum ether and ethyl acetate as the eluent. The two *E* and *Z* isomers were isolated in roughly equivalent quantities. Each *E*-TPE-2OH or *Z*-TPE-2OH isomer was reacted using an excess of tosyl chloride and triethylamine in dichloromethane, providing the two desired ditosylated *E*-TPE-2OTs and *Z*-TPE-2OTs initiators **3**.

The synthesis of TPE derivatives is well documented, but the separation and purification of stereoisomers can be challenging depending on the nature of the substituents. Zhang and colleagues studied disubstituted TPE derivatives, and found that *E* and *Z*-TPE derivatives with polar substituents such as oxazolyl and pyridyl groups were easily separated by column chromatography, while TPE substituted with apolar groups such as benzene and naphthalene showed only one spot on TLC, making purification impossible.[40] In our case, the first *E* and *Z*-TPE derivatives **1** could not be separated due to the low polarity of the phenol unit. However, extending the side chains with two hydroxyethoxy groups significantly increased their polarity. The free rotation of the side chains and the primary hydroxy end-group created sufficient differences in the dipole moments, enabling the separation of the isomers. Both *E* and *Z*-TPE-2OTs exhibited closely positioned but distinguishable spots on the TLC, reflecting the lower polarity of the tosyl groups compared to the previous hydroxethoxy chains (Fig. S7, ESI†). Although both isomers showed identical ^{13}C NMR and mass spectra (Fig. S4 and S5, ESI†), slight differences in proton shifts related to the TPE unit could be observed from ^{1}H NMR (Fig. 1).

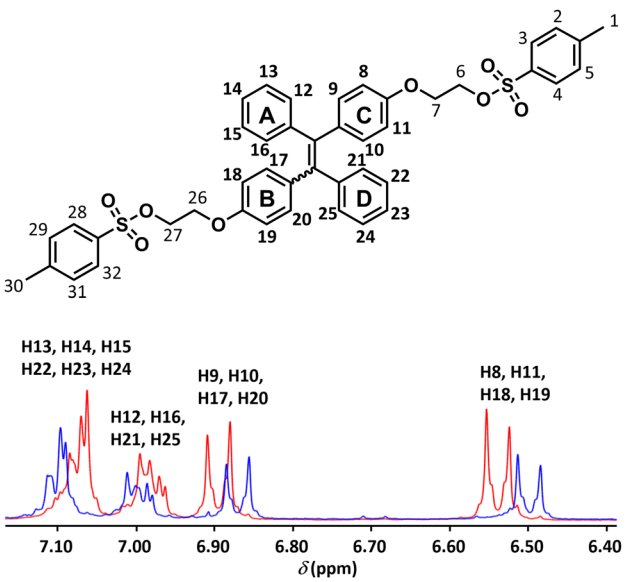

Fig. 1 Overlay of the ^{1}H NMR spectra of both *E*-TPE-2OTs (blue spectra) and *Z*-TPE-2OTs (red spectra), depicting the effect of TPE configuration on the chemical shifts of aromatic protons.

The signals at 6.50 and 6.87 ppm for *E*-TPE-2OTs appear at lower chemical shifts compared to the corresponding peaks for *Z*-TPE-2OTs. The protons associated with these peaks are located on the two substituted rings B and C. For the two peaks at 7.00 and 7.10 ppm, the opposite trend is observed, with the peaks being shifted to slightly higher chemical shift values. These two signals correspond to the protons of the unsubstituted rings A and D. The geometry structures of the *E*/*Z*-isomers were further confirmed by ROESY ^{1}H NMR spectroscopy, which is widely applicable to those structures (Fig. S10, ESI,† for complete spectra). Focusing on the TPE region as shown in Fig. 2, the resonance peak at 6.50 ppm is easily attributed to H8, H11, H18 and H19 due to their strong correlation with H7 and H26. Similarly, the signal at 6.81 ppm is assigned to H9, H10, H17 and H20 on account of their strong correlation with H8, H11, H18 and H19 for both isomers. The peaks at 6.94 and 7.03 ppm are attributed to H12, H16, H21, H25 and H13, H14, H15, H22, H23 and H24, respectively. Moreover, a weak correlation (highlighted by the two red circles) can be observed between H9, H10, H17, H20 and H12, H16, H21, H25 for *E*-TPE-2OTs (Fig. 2A), while this correlation is not present for *Z*-TPE-2OTs (Fig. 2B). This suggests that for *E*-TPE-2OTs, the A and D rings lie in the same plane as the B and C rings, accounting for the spatial proximity of the protons. On the other hand, in the case of *Z*-TPE-2OTs, the A and D rings are not coplanar with the B and C rings, resulting in the absence of proton correlation. Hence, the *E*/*Z*-configurations directly influence the conformation of the substituted rings. Specifically, in the *Z*-configuration, the substituted B and C rings rotate out of the plane to minimize the steric hindrance caused by the two bulky tosyl groups. In contrast, in the *E*-configuration, the substituents do not interact with each other, suggesting that all four TPE rings remain coplanar in solution. X-ray diffraction is the most powerful technique for determining both configurations.[41] While repeated attempts to obtain single crystals for any of the TPE-2OTs isomers were unsuccessful, crystallization of *E*/*Z*-TPE-2OH was achieved (Fig. 3). The single crystal structures were obtained by slow evaporation of pure *E*/*Z*-TPE-2OH in a mixture of acetone and ethyl acetate. The single crystal X-ray diffraction analyses clearly show the chemical structure of both *E*/*Z*-TPE-2OH isomers, thus confirming the configurations determined by ROESY. It is worth noting that some hydroxy groups are disorganized in the crystal lattice, which originates from the intermolecular hydrogen bonds with other TPE-2OH and water molecules in the case of *Z*-TPE-2OH (Fig. S9, ESI†).

Synthesis and characterization of *E*/*Z*-copolymers

Building on the successful synthesis of each *E*/*Z*-TPE-2OTs isomer, amphiphilic triblock copolymers *E*/*Z*-TPE-P*n*BuOx-*b*-(P*n*PrOx-*stat*-PMeOx), simplified as *E*/*Z*-copolymers, were subsequently synthesized *via* CROP using these isomers as initiators (Scheme 2). The synthesis began with the introduction of 2-*n*-butyl-2-oxazoline (*n*BuOx) to form the hydrophobic block. Then, 2-*n*-propyl-2-oxazoline (*n*PrOx) and 2-methyl-2-oxazoline (MeOx) were added at once to create the desired hydrophilic block. Finally, the polymerization was terminated by adding a

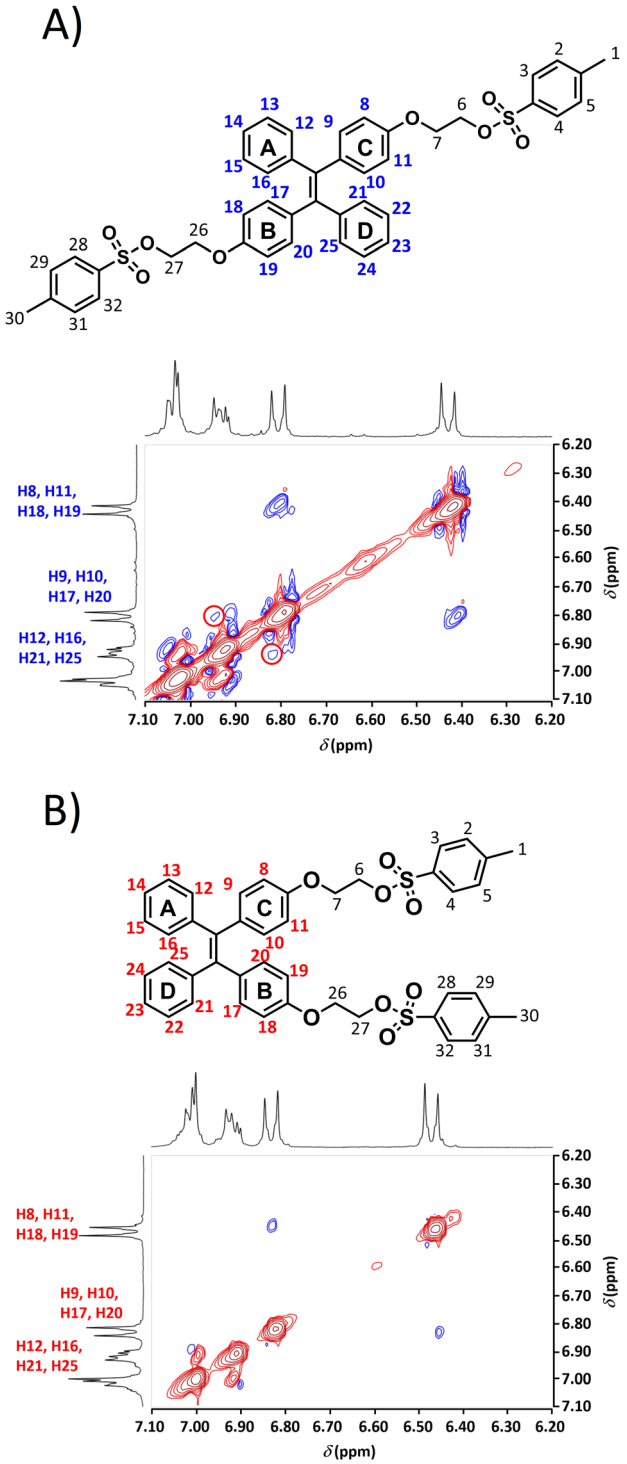

Fig. 2 Partial ROESY ^{1}H NMR spectra of (A) *E*-TPE-2OTs and (B) *Z*-TPE-2OTs, displaying the spatial correlations between the aromatic protons of TPE. The red circles highlight the weak correlation between specific protons that confirm the *E*/*Z*-configurations.

5 M solution of KOH in MeOH. The rational design behind such copolymer was to first achieve self-assembly properties in an aqueous medium to form micelles. Thus, the proportions between the hydrophobic and hydrophilic blocks were wisely

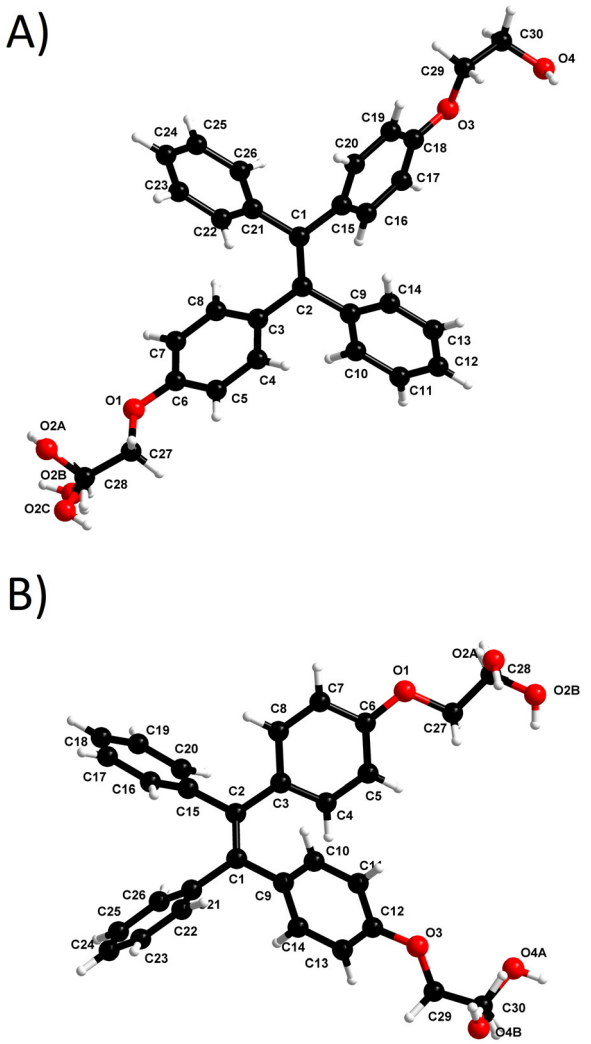

Fig. 3 Single crystal structures of (A) *E*-TPE-2OH and (B) *Z*-TPE-2OH determined by X-ray diffraction.

selected to obtain a final copolymer with a hydrophilic-lipophilic balance (HLB) superior to 10 for an oil-in-water system favoring micellization.[42] P*n*BuOx was selected because of its high hydrophobicity, while PMeOx is well known for its high water solubility. Since neither polymer undergoes phase transition behavior in water between 0 and 100 °C, poly(2-*n*-propyl-2-oxazoline) (P*n*PrOx) was introduced to provide thermo-responsiveness and intermediate water solubility. Although the LCST of P*n*PrOx is relatively low (~25 °C),[13] the copolymerization with MeOx aims to increase the LCST value which correlates with the initial *n*PrOx : MeOx (7 : 3) mole ratio. Therefore, the proportion between both monomers was carefully determined to balance the LCST behavior, while maintaining the self-assembly properties. Both *E*/*Z*-TPE-2OTs successfully initiated the polymerization of 2-oxazolines as depicted by ^{1}H NMR, affording the desired copolymers (Fig. S11 and S12, ESI†). The aromatic region is clearly visible from 6.54 to 7.13 ppm, indicating the presence of TPE in both cases. Concerning the copolymer spectral region, the triblock composition makes

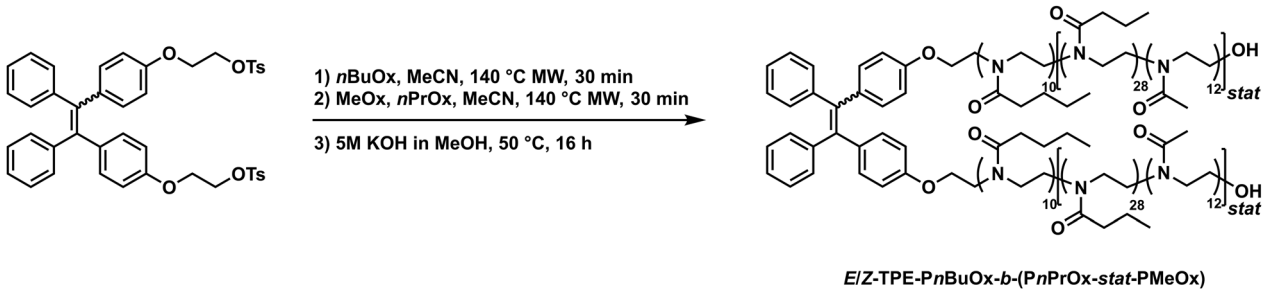

Scheme 2 Synthesis of hydroxy terminated *E*/*Z*-TPE-P*n*BuOx-*b*-(P*n*PrOx-*stat*-PMeOx) copolymers by successive polymerization of *n*BuOx, and statistical copolymerization of MeOx and *n*PrOx using *E*/*Z*-TPE-2OTs as the initiator.

Table 1 Characterization of *E*/*Z*-copolymers by SEC[a]

Copolymer	M_n (theor.), g mol^{-1}	M_n (exp.), g mol^{-1}	$Đ$
E	11 376	10 700	1.59
Z	11 376	9300	1.63

[a] Determined by SEC in DMF using PMMA as the standard.

it difficult to accurately determine the degree of polymerization of each block by ^{1}H NMR. However, the total amount of protons is consistent with the expected theoretical value (Table 1), indicating that all the monomers were consumed during the polymerization reaction. The number-average molar mass M_n was obtained by size-exclusion chromatography (SEC). Given the theoretical value M_n(theor.) = 11 376 g mol^{-1}, the experimental M_n were slightly lower, with dispersities of 1.59 and 1.63 for the *E* and *Z*-copolymers, respectively. CROP requires rapid and uniform generation of carbocationic chain ends, as slow or heterogeneous initiation results in broader dispersity and lower M_n. Hoogenboom *et al.* demonstrated that using ethyl tosylate instead of methyl tosylate in CROP increased the dispersity due to its slower initiation kinetics. This difference is explained by a less electrophilic and bulkier initiator, leading to a slower initiator step, which ultimately favors side reactions by chain transfers during the propagation step. The slightly higher M_n observed for the *E*-isomer initiator can be attributed to its more favorable initiation compared to the sterically hindered *Z*-isomer, leading to more efficient chain propagation and, consequently, lower dispersity.[43]

TPE derivatives are known to undergo thermal isomerization when exposed to high temperature.[44,45] Therefore, the thermal stability of both *E*/*Z*-TPE-2OTs isomers was studied by ^{1}H NMR under the polymerization conditions in the absence of monomers (Fig. S13, ESI†). After heating at 140 °C in acetonitrile for 30 min, both *E* and *Z*-isomers showed approximately 10% degradation, as evidenced by the appearance of new signals at lower chemical shifts compared to those of TPE-2OTs. While the degradation percentage was relatively low and identical for both isomers, their thermal behavior exhibited significant differences. As a matter of fact, while the *Z*-TPE-2OTs isomer showed an isomerization rate of up to 10%, its *E*-TPE-2OTs counterpart exhibited a significantly higher conversion rate, reaching 43%. Leigh and Arnold investigated the thermal isomerization of different TPE derivatives and demonstrated that the isomerization of *para*-dimethoxytetraphenylethylene occurs much faster in polar solvents such as benzonitrile than in apolar solvents such as benzene. Furthermore, the authors mentioned that the *Z*-isomer is more thermally stable in benzonitrile.[46] In the case of TPE-2OTs, the higher isomerization rate of the *E*-isomer can be attributed to the polar nature of acetonitrile. While the *E*/*Z*-TPE-2OTs initiators demonstrated clear isomerization under polymerization conditions, it is important to note that the resulting polymers showed no evidence of such phenomenon. Indeed, the ^{1}H NMR spectra of the TPE units from both *E* and *Z*-copolymers exhibit chemical shift patterns that are identical to those of their respective initiators (Fig. S14, ESI†). This observation confirms that no mixture of *E* and *Z*-polymers was formed during the synthesis, suggesting that the polymerization of 2-oxazolines effectively prevents the thermal isomerization of the TPE unit. It can be hypothesized that the polymerization reaction is kinetically faster than the isomerization process. In fact, microwave-assisted CROP of oxazolines are known to be extremely fast.[47] Additionally, we assume that the TPE configuration is locked by the bulky brush-like POx chain structure, which restricts rotation and prevents isomerization of the TPE unit.

Self-assembly of *E*/*Z*-copolymers

The *E*/*Z*-copolymers were successfully dispersed in phosphate buffered saline (PBS, pH = 7) to form micelles using the thin film hydration method. As shown in Fig. 4, the initial hydrodynamic diameters (D_h) were measured to be 41 and 37 nm for the *E* and *Z*-micelles, respectively. Additionally, narrow size distributions were achieved, as indicated by the low polydispersity index (PDI) (Table S1, ESI†). The colloids displayed good stability, although aggregation was observed over time. This was evidenced by an increase in both D_h and PDI over time for the micelles, suggesting the formation of aggregates. At identical copolymer concentrations (10 mg mL^{-1}), the *Z*-copolymer self-assembled into smaller micelles (D_h = 37 nm) compared to the *E*-copolymer (D_h = 41 nm). This difference can be attributed to the distinct configurations of the TPE unit in the copolymers. In the *E* configuration, the copolymer chains are positioned on opposite sides of the TPE unit, forcing interwoven packing of the amphiphile parts in the aggregated state. This increases the core volume of the micelles. Conversely, the *Z*-configuration

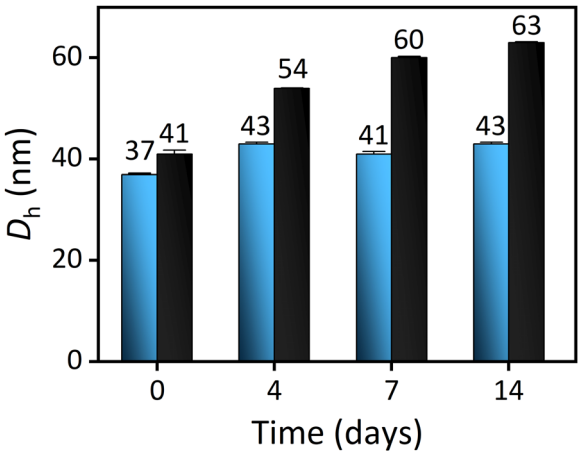

Fig. 4 Evolution of the hydrodynamic diameter of *E*-micelles (black bars) and *Z*-micelles (blue bars) over 14 days. The samples (c = 10 mg mL^{-1}) were stored 4 °C. The indicated numbers on each bar represent the average hydrodynamic diameter (nm). The error bars represent the mean standard deviation (n = 4).

places the copolymer chains on the same side of the TPE unit, facilitating a more efficient micellization process and resulting in smaller micelles. Importantly, the *Z*-micelles showed minimal aggregation, as depicted by the negligible increase of the D_h and PDI in comparison with the *E*-micelles. Indeed, while both *E*/*Z*-micelles showed aggregation over time, the *Z*-micelles could be effectively redispersed using ultrasound, unlike the *E*-micelles. The measured D_h and PDI of the *Z*-micelles remained constant over two weeks, whereas the *E*-micelles could not be redispersed and demonstrated irreversible aggregation.

AIE behavior of *E*/*Z*-copolymers

The AIE behavior of *E*/*Z*-copolymers was studied by fluorescence at a concentration of 1 mg mL^{-1} in THF:water mixtures with varying water fractions (f_w) (Fig. 5A and B). Both copolymers showed a weak fluorescence at λ_{max} = 385 nm in THF, which corresponds to the emission of solubilized TPE. With the increasing of the water fraction, the emission band at 385 nm diminished and the characteristic fluorescence of the aggregated TPE appeared at λ_{max} = 475 nm and 481 nm for the *E* and *Z*-copolymers, respectively. This phenomenon was noticeable when f_w reached 80% and was further visible at f_w = 90% and 100%. Although both copolymers exhibited AIE properties starting from f_w = 80%, the *Z*-copolymer was slightly more emissive than the *E*-copolymer at f_w > 80% (Fig. S15, ESI†). Indeed, the relative fluorescence quantum yield was determined to be 0.12 and 0.16 for the *E* and *Z*-copolymers, respectively, in agreement with reported values for other TPE-based copylmers.[32,48] In fact, differences in the fluorescence properties between *E*/*Z*-TPE derivatives have been previously described.[45,49] As a result of the AIE properties, the critical micellar concentration (CMC) of the *E*/*Z*-copolymers was determined by fluorescence. Indeed, owing to the specific emission of TPE at $\lambda_{max} \approx$ 480 nm, the CMC can be calculated by varying the concentration of the copolymer in an aqueous media. CMC values of 0.53 and 0.06 μg mL^{-1} were found for the *E* and *Z*-copolymers, respectively (Fig. 5C and D). The low CMC values are attributed to the strong AIE properties of TPE and the amphiphilic nature of the copolymer, both of which facilitate rapid aggregation in aqueous media. These two effects work synergistically to favor the self-assembly of the copolymers. Interestingly, it is worth noting that the CMC for the *Z*-copolymer is ∼10-fold lower than that for the *E*-copolymer. This difference is likely an immediate consequence of the difference in the configuration of TPE. Indeed, in the case of the *Z*-copolymer, the structure of the hydrophobic block is such that the aggregation of TPE is easier compared to the *E*-copolymer, in which the P*n*BuOx chains from both sides of TPE could hinder the aggregation of the latter during the micellization process. Since micelles are dynamic supramole cular assemblies in equilibrium with their unimers, a low CMC is particularly advantageous as micelles are prone to dissociation upon high dilution. Hence, in addition to the fluorescent properties, the presence of TPE also contributes to the colloidal stability of the micelles. The calculated CMC of the *Z*-micelles was found to be lower by a factor of 10 compared to that of the *E*-micelles, indicating that the micellization process occurs more rapidly for the *Z*-copolymer than for the *E*-copolymer. This result corroborates previous observations related to the colloidal stability and AIE properties of both copolymers.

Thermoresponsiveness of *E*/*Z*-copolymers

The heat responsiveness of micelles was studied by turbidity using UV-Vis spectroscopy. Colloidal solutions of *E*/*Z*-micelles (c = 1 mg mL^{-1}) were gradually heated (1 °C/5 min), and transmittance was monitored at 600 nm (Fig. 5F and G). The cloud point temperature, T_{cp}, defined as the temperature at which turbidity occurs at a given concentration, was measured to be 40 °C and 38 °C for the *E* and *Z*-copolymers, respectively. The 2 °C difference may result from small variations in the copolymer composition, as shown by the SEC measurements, where different numbers for the average molar mass were obtained. A slight change in the hydrophilic block during the copolymerization of the *n*PrOx and MeOx monomers could lead to these differences in T_{cp}. Nonetheless, T_{cp} is above 37 °C, which corresponds to the body temperature for both *E*/*Z*-micelles, making them potentially useful for thermal drug delivery systems.

Encapsulation of DiI and NBDHEX in *E*/*Z*-micelles

To explore the potential of both E and Z-micelles for imaging and therapy, two lipophilic molecules were selected. 1,1′-Dioctadecyl-3,3,3′,3′-tetramethylindocarbocyanine perchlorate (DiI) was chosen for its high extinction coefficient and moderate fluorescence quantum yield, which enable its detection even at very low concentrations. Moreover, since *E*/*Z*-copolymers emit a broad fluorescence signal at λ_{max}(em) ≈ 480 nm, a FRET pair could be obtained with the *E*/*Z*-copolymer as the donor and DiI as the acceptor (λ_{max}(abs) = 550 nm, Fig. S16, ESI†). NBDHEX was selected as an anticancer agent

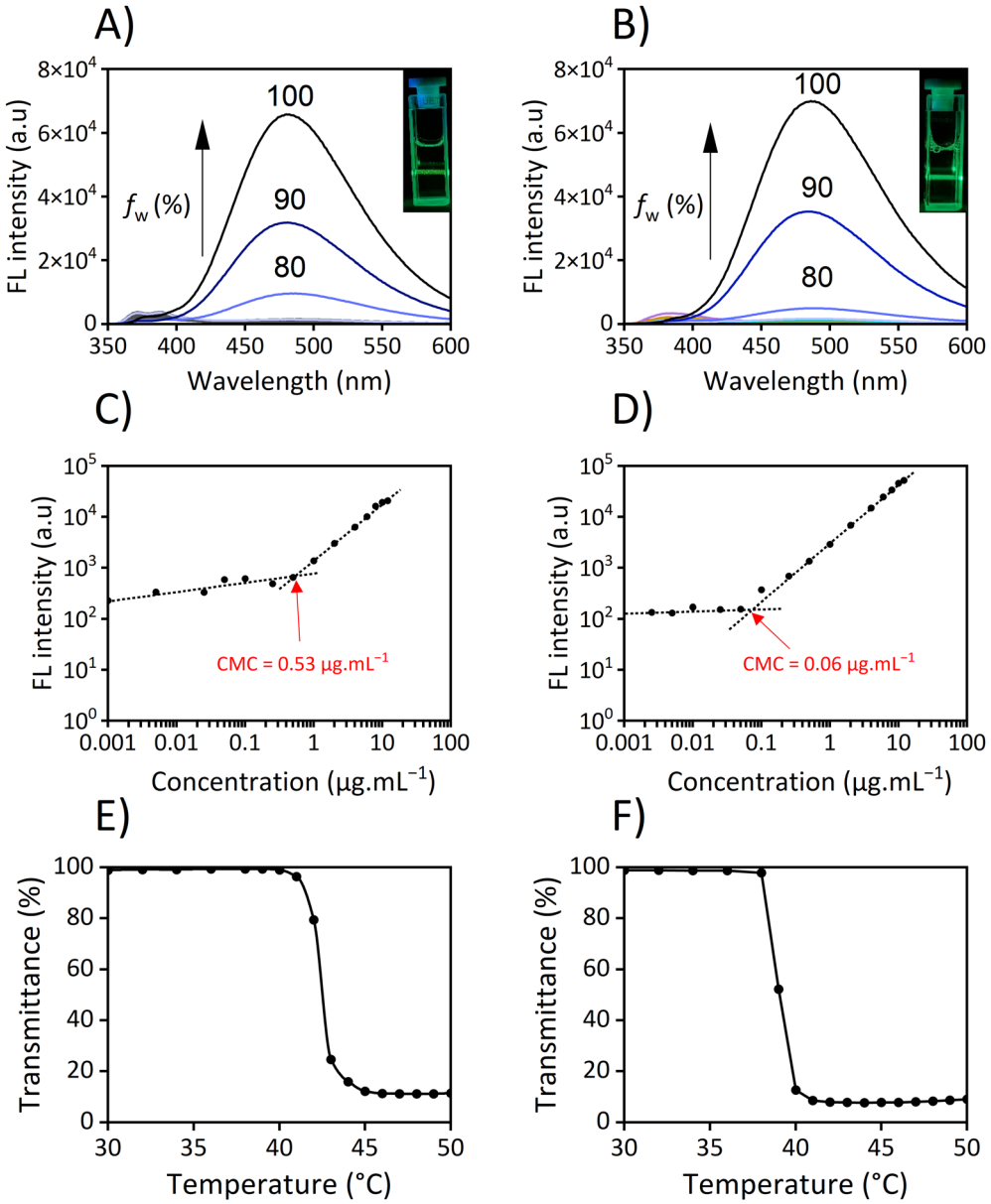

Fig. 5 Physico-chemical properties of *E*/*Z*-copolymers: the water dependence aggregation-induced emission for (A) *E*-copolymer and (B) *Z*-copolymer; insets show the Tyndall effect in water at c = 1 mg mL^{-1}; the CMC values of (C) *E*-copolymer and (D) *Z*-copolymer; the cloud point temperature of (E) *E*-copolymer and (F) *Z*-copolymer in water at c = 1 mg mL^{-1} by turbidimetry using UV-Vis spectroscopy in transmission mode at λ = 600 nm with a rate of 1 °C/5 min.

due to its strong inhibition of the glutathione *S*-transferase P1-1 (GSTP1-1), which is known to induce cell apoptosis.[50] NBDHEX was synthesized in one step starting from the commercially available 4-chloro-7-nitrobenzofurazan (NBDCl) by reacting with 6-mercapto-1-hexanol (Scheme S1, ESI†). The desired product NBDHEX was obtained, as confirmed by ^{1}H NMR and mass spectrometry (Fig. S6, ESI†). DiI and NBDHEX were successfully encapsulated into *E*/*Z*-micelles using the thin film hydration method, providing DiI@*E*/*Z*-micelles and NBDHEX@*E*/*Z*-micelles (Fig. 6A and B). UV-Vis spectroscopy revealed the characteristic absorption bands of DiI (λ_{max} = 550 nm), NBDHEX (λ_{max} = 420 nm) and TPE (λ_{max} = 320 nm), confirming the presence of DiI and NBDHEX in the micelles. The concentrations of encapsulated DiI and NBDHEX were determined by UV-Vis spectroscopy using a calibration curve (Fig. S17, ESI†). The encapsulation efficiencies (EE) for DiI@*E*/*Z*-micelles were generally higher than those for NBDHEX (Table S2, ESI†). This noticeable difference between DiI and NBDHEX is likely due to the greater lipophilic nature of DiI, which facilitates interactions with TPE *via* π-stacking, enhancing its encapsulation and retention within the micelle core during the formulation. Nonetheless, no significant differences in terms of encapsulation efficiency between the *E*/*Z*-micelles were observed. The encapsulation of DiI and NBDHEX only

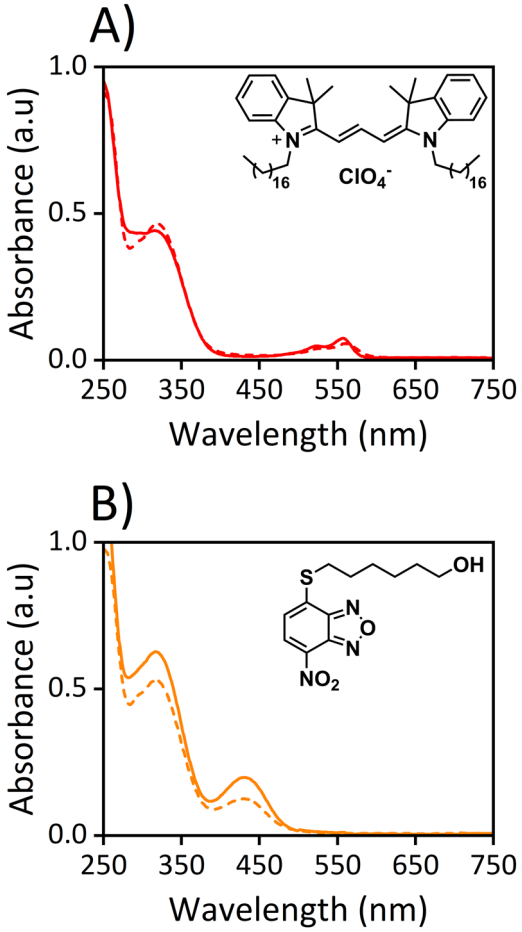

Fig. 6 UV-Vis spectra in PBS (1 mg mL^{-1}) of *Z*-micelles (dashed lines) and *E*-micelles (plain lines) containing either (A) DiI or (B) NBDHEX.

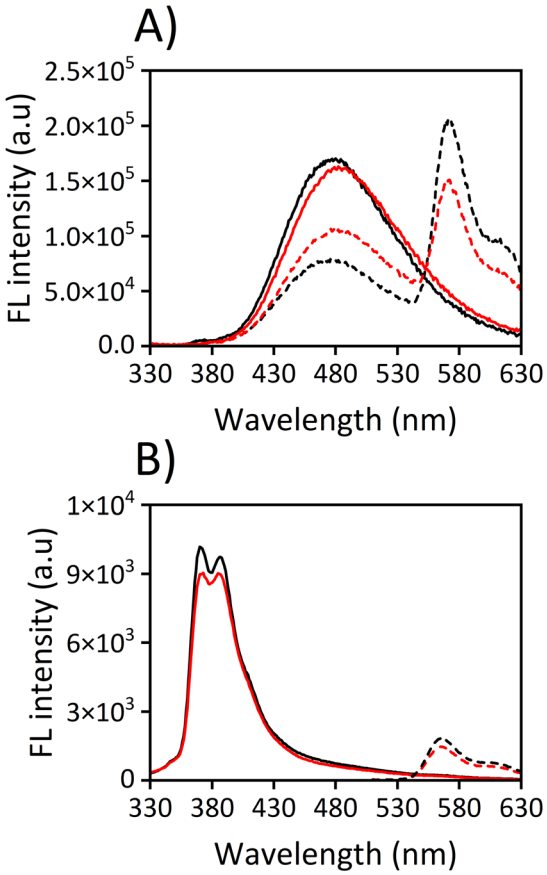

Fig. 7 FRET study of DiI@*E*/*Z*-micelles. (A) Emission spectra of empty *E*/*Z*-micelles (black/red, plain lines) and DiI@*E*/*Z*-micelles (black/red, dashed lines) when excited at λ_{exc} = 320 nm. (B) Emission spectra of the diluted solutions of DiI@*E*/*Z*-micelles in MeOH when excited at λ_{exc} = 320 nm (black/red, plain lines) and λ_{exc} = 500 nm (black/red, dashed lines).

showed minor modifications in the nanoparticle size, as measured by DLS (Fig. S18 and Table S1, ESI†).

Förster resonance energy transfer in DiI@*E*/*Z*-micelles

A FRET pair is observed between a donor and acceptor when their respective emission and absorption spectra significantly overlap. Moreover, the donor must be in close proximity to the acceptor (d = 1–10 nm) to transfer the energy from the excited state to the acceptor in its ground state.[51] Micelles are particularly suitable for FRET due to their small hydrophobic core, which promotes close proximity and energy transfer between the donor and the acceptor. In our study, *E*/*Z*-micelles, with sizes around 40 nm, were expected to have a suitable hydrophobic core to facilitate FRET by encapsulating DiI. TPE (donor) and DiI (acceptor) exhibit significant spectral overlap between the AIE emission of TPE and the absorption of DiI. Thus, FRET of DiI@*E*/*Z*-micelles was studied by fluorescence (Fig. 7A). Upon excitation at 320 nm, the AIE emission band of TPE with the maximum at ∼480 nm decreased for both DiI@*E*/*Z*-micelles compared to their respective empty micelles at the same concentration (c = 1 mg mL^{-1}), followed by the appearance of the characteristic emission band of DiI with the maximum at 575 nm. The FRET efficiency (E_{FRET}) was determined to be 54% and 34% for DiI@*E*-micelles and DiI@*Z*-micelles, respectively. Both systems were promising, as most of the encapsulated DiI emitted fluorescence by FRET (Fig. S19, ESI†). To further confirm the encapsulation of DiI inside the hydrophobic core of the micelles, a colloidal solution of DiI@*E*/*Z*-micelles was diluted in methanol, inducing micelle disassembly (Fig. 7B). When excited at 320 nm, neither the AIE of TPE nor emission of DiI *via* FRET was observed. Instead, only the emission with the maximum at 385 nm, corresponding to solubilized TPE, was detected. The absence of the AIE band indicates that the micelles had disassembled into soluble unimers, rendering FRET impossible. The presence of unencapsulated DiI in the resulting solutions was confirmed by excitation at 500 nm, which gave the characteristic emission of DiI. This result validates the successful encapsulation of DiI within the micelles and the occurrence of FRET between TPE and DiI. Such micelles could be used for dual imaging, tracking micelles *via* AIE from TPE and FRET-based fluorescence probes.

Cellular toxicity of *E*/*Z*-micelles

The ability of *E*/*Z*-micelles to deliver hydrophobic molecules was assessed against the HeLa cancer cell line using

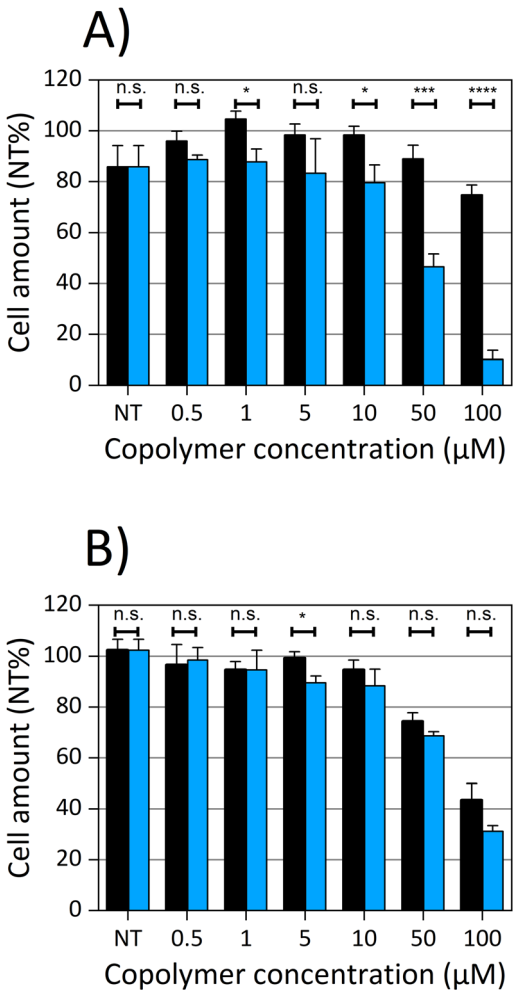

Fig. 8 Cell proliferation/survival assay at 37 °C for (A) *E*-micelles and (B) *Z*-micelles without (black bars) and loaded with NBDHEX (blue bars). NT refers to 'not treated' cells (control). Student's *t*-test (*$p \leq 0.05$; ***$p \leq 0.001$; ****$p \leq 0.0001$; n.s. = not significant).

NBDHEX@*E*/*Z*-micelles (Fig. 8). Cells were treated with *E*/*Z*-micelles with concentrations of copolymer ranging from 0.5 to 100 μM. Firstly, the cells treated with *E*-micelles showed no significant effect on the cell proliferation at all concentrations (Fig. 8A, black bars). However, a dose-dependent decrease in the measured cell amount was observed with *Z*-micelles (Fig. 8B, black bars), with only 44% of the remaining cells at 100 μM. When treated with NBDHEX@*E*-micelles, the cell amount significantly decreased at concentrations from 50 to 100 μM, with only 10% of the remaining cells at 100 μM. Surprisingly, NBDHEX@*Z*-micelles induced only a slight decrease in cell proliferation compared to the *Z*-micelles at the same concentrations. These results suggest that *Z*-micelles are not able to deliver the cargo within the cells as opposed to the *E*-micelles, which clearly demonstrate a strong decrease in cell proliferation when loaded with NBDHEX. Therefore, we assumed that the *Z*-micelles were not stable in the biological media to be internalized and to deliver NBDHEX within the cytoplasmic compartment. Following this hypothesis and assuming that the micelles are mostly disassembled into unimers in the biological media, the hydrophobic part of the copolymer may interact with the cell membrane, leading to physical modifications, loss of membrane integrity and ultimately to cell death, as reported for various lipophilic compounds.[52]

In parallel, the same experiment was performed by heating the cells at 41 °C for 5 min after 2 h post-treatment to study the influence of the thermoresponsiveness of the *E*/*Z*-micelles in the release of NBDHEX (Fig. S20, ESI†). The increase in temperature to 41 °C proved to be harmless to the cells, as shown by the control condition. However, no additional decrease in cell survivability was observed for both NBDHEX@*E*/*Z*-micelles. It was expected that crossing the cloud point temperature of both *E*/*Z*-micelles would lead to their destabilization, which would accelerate the release of the hydrophobic cargo. This strongly suggests that the micelles are not stable when reaching the cytoplasmic compartment, which most likely leads to their disassembly and immediate release of NBDHEX. In this scenario, heating above the cloud point temperature would have no additional effect on the release of NBDHEX.

To further study the delivery of a hydrophobic cargo, HeLa cells were also treated with DiI@*E*/*Z*-micelles and the fluorescence of TPE, DiI and FRET emission were measured (Fig. 9). The cells were treated for 2 h, and then thoroughly washed to eliminate the excess of extracellular micelles before fluorescence acquisition. When excited at ~320 nm (Fig. 9A), the fluorescence of cells treated with *E*-micelles exhibited a significant increase, owing to the AIE of TPE. No detectable fluorescence enhancement was observed for either *Z*-micelles or DiI@*Z*-micelles conditions. In the case of DiI@*E*-micelles, the detected emission was much lower than that of *E*-micelles due to the FRET phenomenon, which resulted in the decrease of the AIE due to energy transfer. When excited at ~550 nm (Fig. 9B), a strong fluorescence signal could be observed in cells treated with DiI@*E*-micelles, indicating the penetration of DiI within the cells. However, no additional fluorescence could be detected in cells treated with DiI@*Z*-micelles, which was consistent with the lack of AIE from TPE when excited at 320 nm under the same condition. This strongly suggests that the *Z*-micelles did not penetrate the cells and were washed away during the treatment. Indeed, when exciting at ~320 nm and measuring the fluorescence at ~620 nm (Fig. 9C), a 2.5-fold increase in fluorescence relative to the not treated cells was measured for DiI@*E*-micelles, while no additional emission from DiI@*Z*-micelles was detected. Since FRET requires both donor and acceptor to be close from each other, these results indirectly demonstrate that the *E*-micelles are effectively internalized as opposed to the *Z*-micelles. Even though no DiI was present in cells treated with *E*-micelles, the broad emission from AIE of TPE was still detected, thus explaining the apparent increase in fluorescence. To ensure the result discrepancy obtained with *E* and *Z*-micelles did not originate from micelle degradation, the AIE, DiI and FRET emission of each micelle in solution (without cells or biological media) were quantitated concurrently to biological experiment, and no anomaly was

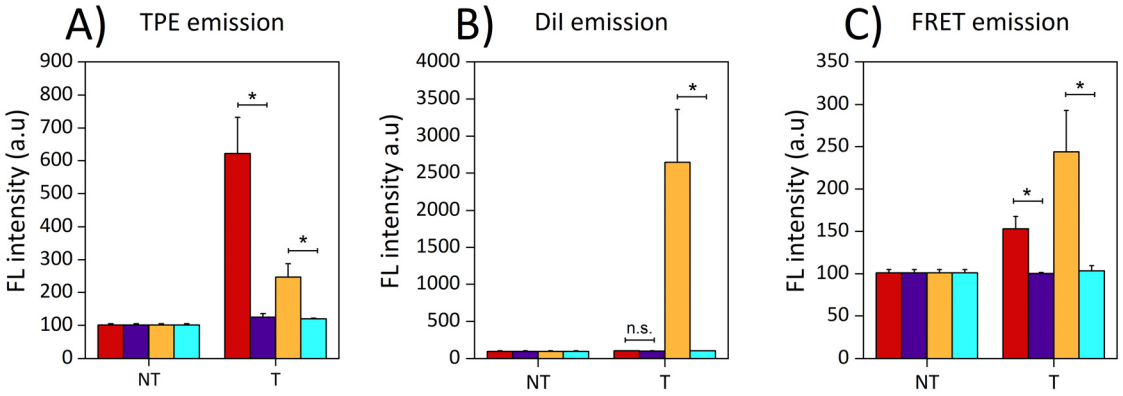

Fig. 9 HeLa cells were treated with *E*-micelles (red bars), *Z*-micelles (purple bars), DiI@*E*-micelles (yellow bars) and DiI@*Z*-micelles (cyan bars). Each chart represents the total fluorescence at different excitation and detected emission wavelengths: (A) AIE from TPE (λ_{exc} = 324–326 nm; λ_{em} = 440–470 nm); (B) DiI emission (λ_{exc} = 528–554 nm; λ_{em} = 604–640 nm); (C) FRET emission (λ_{exc} = 324–326 nm; λ_{em} = 604–640 nm). 'NT' and 'T' conditions refer to 'not treated' (control) and 'treated' cells, respectively. Student's *t*-test (*$p \leq 0.05$; n.s. = not significant).

noticed (Fig. S21, ESI†). These results are in agreement with the cytotoxicity study and further support the inability of *Z*-micelles to penetrate the cell membrane and deliver hydrophobic molecules.

Experimental section

Materials

Reagents. All chemicals were used without further purification unless specified otherwise. Zinc powder (Zn, ≥99%), 2-chloroethanol (99%), tosyl chloride (TsCl, ≥98%), triethylamine (Et_3N, ≥99.5%), potassium iodide (KI, ≥99%), 6-mercapto-1-hexanol (97%), 2-methyl-2-oxazoline (MeOx, 97%), 2-*n*-propyl-2-oxazoline (*n*PrOx), 2-*n*-butyl-2-oxazoline (*n*BuOx) and phosphate buffered saline (PBS) tablets were purchased from Sigma Aldrich. Dichloromethane (CH_2Cl_2, 99.8%), acetonitrile (ACN, ≥99%), *N*,*N*-dimethylformamide (DMF, 99.8%), potassium carbonate (K_2CO_3, ≥99%), 4-chloro-7-nitrobenzofurazan (NBDCl, 98%), 1,1′-dioctadecyl-3,3,3′,3′-tetramethylindocarbocyanine perchlorate (DiI), petroleum ether (PE, ≥99%), ethyl acetate (EtOAc, ≥99%) and chloroform ($CHCl_3$, ≥99%) were obtained from Thermo Fisher Scientific. 4-Hydroxybenzophenone (≥98%) was purchased from TCI. Titanium tetrachloride ($TiCl_4$, 97%) was obtained from Merck. Diethyl ether (Et_2O) was purchased from VWR. Tetrahydrofuran (THF, ≥99%) was obtained from Thermo Fisher Scientific, and distilled over sodium and benzophenone. Dicalite was obtained from Carlo Erba. Column chromatography was carried out on Kieselgel 60 A (0.035–0.070 mm mesh, Thermo Fischer Scientific).

Instrumentation. The synthesis of copolymers was carried out using a microwave reactor (Anton Paar Monowave 400). Sonication was realized using a FB11203 Fisherbrand® apparatus (37 kHz, power 100%, pulse). ^{1}H NMR and ^{13}C NMR spectra were recorded using 300 MHz and 500 MHz Bruker Aspect spectrometers, respectively. Chemical shifts (δ) are given in parts per million relative to the NMR solvent residual peak ($CHCl_3$, δ = 7.26 ppm). UV-Vis spectroscopy measurements were recorded on a Shimadzu UV-1800 spectrophotometer using a quartz cell of 1 cm path length. Fluorescence spectra were recorded on a Shimadzu RF-6000 spectrophotometer using a quartz cell of 1 cm path length.

The molar masses (number-average molar mass M_n, weight-average molar mass M_w) and dispersity ($Đ$) values of the poly(2-ozaxoline)s were measured by SEC using DMF with LiBr (1 g L^{-1}) as an eluent, and carried out using a system equipped with an isocratic HPLC pump (Waters 1515), a Waters 2707 plus autosampler, with a guard column (PL gel, 5 μm Guard column, 8 × 50 mm), followed by two columns (PL gel, linear 5 μm, 8 × 300 mm), with all three columns stored in an oven at 60 °C, with a photodiode array (Waters 2998) detector and a differential Waters 2414 refractometer at 40 °C. The instrument operated at a flow rate of 1.0 mL min^{-1} at 35 °C, and was calibrated with narrow linear poly(methyl methacrylate) (PMMA) standards ranging in molar mass from 0.904 kg mol^{-1} to 304 kg mol^{-1}.

Matrix adsorption laser desorption ionization time of flight (MALDI-TOF) measurements were performed on a SPIRAL-TOF S3000 from JEOL using trans-2-[3-(4-*tert*-butylphenyl)-2-methyl-2-propenylidene]malononitrile (DCTB) as matrix.

Dynamic light scattering measurements were performed using a Malvern Zetasizer Nano S.

Melting points (m.p.) were determined using a Stuart SMP30 apparatus.

X-ray diffraction analyses were performed on a Rigaku Oxford Diffraction SuperNova diffractometer equipped with an Atlas CCD detector and micro-focus Cu-K$_\alpha$ radiation (λ = 1.54184 Å). The structures were solved by dual-space algorithm and refined on F^2 by full matrix least-squares techniques using the SHELX package (G. M. Sheldrick, ShelXT-2018/2, ShelXL-2019/3). All non-hydrogen atoms were refined anisotropically and the H atoms were included in the calculation without refinement. Absorption was corrected with multiscan empirical method or Gaussian technique by using the CrysAlisPro program (CrysAlisPro, Rigaku Oxford Diffraction, V1.171.44.99a, 2025).

Preparation of DiI and NBDHEX@*E*/*Z*-micelles

Organic synthesis. Compound (**1**) was prepared in accordance with the literature.[31]

^{1}H NMR (300 MHz, $CDCl_3$) δ (ppm): 7.16–6.84 (m, 14H), 6.56 (m, 4H). ^{13}C NMR (500 MHz, $CDCl_3$) δ (ppm): 153.9, 144.1, 139.7, 136.7, 132.7, 131.4, 129.6, 128.4, 128.2, 127.7, 127.6, 126.2, 125.8, 115.0, 114.6. ESI-MS was calculated for 364.15 and found 364.20 $[M]^+$.

Synthesis of *E*/*Z*-TPE-2OH (2). K_2CO_3 (1.8 g, 13.2 mmol, 10 equiv.), KI (219 mg, 1.3 mmol, 1 equiv.) and 2-chloroethanol (446 μL, 6.7 mmol, 5 equiv.) were successively added to a solution of compound **1** (484 mg, 1.3 mmol, 1 equiv.) in anhydrous DMF (10 mL). The mixture was vigorously stirred under an argon atmosphere at 80 °C for 18 h. The reaction was cooled down to room temperature and concentrated under reduced pressure. EtOAc was added, followed by a saturated $NaHCO_3$ aqueous solution. The aqueous phase was extracted with EtOAc and the combined organic layers were washed with brine. The organic layers were dried over $MgSO_4$, then filtered and concentrated under reduced pressure. The crude product was purified by silica gel chromatography (PE/EtOAc 3 : 2 to 1 : 4). The product was further purified by solubilization in CH_2Cl_2 and precipitation in PE to afford *E*/*Z*-TPE-2OH **2** (157 mg and 160 mg, respectively), total yield 53%, $R_f(Z)$ = 0.13 and $R_f(E)$ = 0.39 with 1 : 1 EtOAc/$CHCl_3$ as eluent.

E-TPE-2OH. ^{1}H NMR (300 MHz, $CDCl_3$) δ (ppm): 7.19 (m, 6H), 7.04 (m, 4H), 6.93 (m, 4H), 4.00 (m, 4H), 3.91 (m, 4H), 1.97 (m, 2H). ^{13}C NMR (500 MHz, $CDCl_3$) δ (ppm): 157.0, 144.2, 139.7, 136.8, 132.6, 131.4, 129.5, 128.4, 128.2, 127.7, 126.3, 125.8, 114.2, 113.6. MALDI-TOF-MS was calculated for 452.20 and found 452.20 $[M]^+$. M.p.: 205–207 °C.

Z-TPE-2OH. ^{1}H NMR (300 MHz, $CDCl_3$) δ (ppm): 7.07 (m, 6H), 7.02 (m, 4H), 6.96 (m, 4H), 6.68 (m, 4H), 4.03 (m, 4H), 3.93 (m, 4H), 1.99 (m, 2H). ^{13}C NMR (500 MHz, $CDCl_3$) δ (ppm): 157.0, 144.1, 139.7, 136.9, 132.6, 131.4, 129.5, 128.4, 128.1, 127.6, 126.3, 125.8, 114.2, 113.7, 70.0, 61.5. MALDI-TOF-MS was calculated for 452.20 and found 452.10 $[M]^+$. M.p.: 136–140 °C.

Synthesis of *E*/*Z*-TPE-2OTs (3). A solution of compound **2** (*E* or *Z*-TPE-2OH, 157 mg, 0.4 mmol, 1 equiv.), TsCl (1.03 g, 5.4 mmol, 5 equiv.) and Et_3N (750 μL, 5.4 mmol, 5 equiv.) in CH_2Cl_2 (7 mL) was stirred under an argon atmosphere at room temperature for 24 h. The mixture was immediately purified *via* silica gel chromatography (CH_2Cl_2). The obtained product was then precipitated in PE to afford compound **3** as yellow solids (28–51%, $R_f(Z)$ = 0.32 and $R_f(E)$ = 0.42 with CH_2Cl_2 as eluent).

E-TPE-2OTs. ^{1}H NMR (300 MHz, $CDCl_3$) δ (ppm): 7.81 (m, 4H), 7.33 (m, 4H), 7.11 (m, 6H), 7.01 (m, 4H), 6.88 (m, 4H), 4.31 (m, 4H), 4.06 (m, 4H), 2.44 (s, 6H). ^{13}C NMR (500 MHz, $CDCl_3$) δ (ppm): 156.4, 145.0, 144.0, 139.7, 137.0, 132.9, 132.5, 129.9, 129.4, 128.4, 128.2, 128.0, 127.7, 126.3, 144.2, 113.6, 68.2, 65.2, 21.7. MALDI-TOF-MS calculated for 760.22 and found 760.10 $[M]^+$. M.p.: 62–65 °C.

Z-TPE-2OTs. ^{1}H NMR (300 MHz, $CDCl_3$) δ (ppm): 7.80 (m, 4H), 7.34 (m, 4H), 7.07 (m, 6H), 6.99 (m, 4H), 6.91 (m, 4H), 4.32 (m, 4H), 4.09 (m, 4H), 2.44 (s, 6H). ^{13}C NMR (500 MHz, $CDCl_3$) δ (ppm): 156.4, 145.0, 144.0, 139.7, 137.0, 132.8, 132.5, 131.3, 129.9, 129.8, 129.4, 128.4, 128.2, 128.1, 128.0, 127.6, 126.3, 125.8, 114.2, 113.6, 68.2, 65.2, 21.7. MALDI-TOF-MS calculated for 760.22 and found 760.10 $[M]^+$. M.p.: 64–67 °C.

Synthesis of *E*/*Z*-copolymers. A solution of compound **3** (*E* or *Z*-TPE-2OTs, 30 mg, 0.039 mmol, 1 equiv.) and *n*BuOx (100 μL, 0.79 mmol, 20 equiv.) in anhydrous ACN (960 μL) was heated using a microwave reactor at 140 °C and 600 W for a duration of 30 min under an argon atmosphere. After cooling down, the mixture of *n*PrOx (238 μL, 2.1 mmol, 56 equiv.) and MeOx (80 μL, 0.94 mmol, 24 equiv.) were added, and the reaction was heated again under the same conditions. After cooling down to room temperature, a solution of 5 M KOH in MeOH (1 mL) was added, and the mixture was stirred at 50 °C overnight. The solvents were concentrated under reduced pressure and the polymer was precipitated in cold Et_2O to afford the desired product. The copolymer composition was estimated *via* ^{1}H NMR by integrating the proton signals of PMeOx, P*n*PrOx and P*n*BuOx, and using the characteristic peaks of TPE in the aromatic region as reference.

Synthesis of NBDHEX. To a solution of 4-chloro-7-nitrobenzofurazan (400 mg, 2.0 mmol, 1 equiv.) in EtOH/0.1 M phosphate buffer (1 : 1, 40 mL) was added 6-mercapto-1-hexanol (300 μL, 2.2 mmol, 1.1 equiv.). The reaction was stirred at room temperature for 4 h, and the pH was constantly monitored and adjusted to pH = 7 by adding 1 M NaOH dropwise when necessary. The formed yellow precipitate was filtered and washed with water several times. The solid was dried under vacuum, affording NBDHEX as a yellow brownish solid (324 mg, 55%).

^{1}H NMR (300 MHz, $CDCl_3$) δ (ppm): 8.40 (d, 1H, J = 8.1 Hz), 7.14 (d, 1H, J = 8.1 Hz), 3.67 (m, 2H), 3.28 (t, 2H, J = 7.5 Hz), 1.88 (m, 2H), 1.69–1.40 (m, 7H). ^{13}C NMR (500 MHz, $CDCl_3$) δ (ppm): 149.2, 142.5, 142.0, 132.6, 130.7, 120.3, 62.7, 32.4, 31.7, 28.7, 27.9, 25.3. ESI-MS was calculated for 297.08 and found 297.10 $[M]^+$. M.p.: 70–73 °C.

Micelles formulation

Self-assembly into *E*/*Z*-micelles. Micelles were prepared by following the thin film hydration method. *Z* or *E*-copolymer (10 mg) was first solubilized in $CHCl_3$ (1 mL). The solvent was concentrated under reduced pressure to form a thin film on the flask's wall. Then, PBS (1 mL, pH = 7) was added and the mixture was sonicated using an ultrasound bath for 10 min, keeping the temperature bath under 25 °C. The resulting colloid was filtered with a 0.1 μm syringe filter to afford the desired micelles at a concentration of 10 mg mL^{-1}. The samples were stored in the refrigerator at 4 °C.

Encapsulation of DiI and NBDHEX. The encapsulation was performed in a fashion similar to that of the preparation of *E*/*Z* micelles. A solution of DiI (10 μL, 1 mg mL^{-1}) or NBDHEX (100 μL, 1 mg mL^{-1}) in $CHCl_3$ was added to the *E* or *Z*-copolymer (10 mg) solution in $CHCl_3$ (1 mL). The mixture was then concentrated under reduced pressure and 1 mL of PBS was added. DiI@*E*/*Z*-micelles and NBDHEX@*E*/*Z*-micelles were obtained after 10 min sonication and filtration with a 0.1 μm

filter as pink and yellow colloids, respectively. The colloids were stored at 4 °C. The concentration of the encapsulated molecule was determined by UV-Vis spectroscopy.

The encapsulation efficiency (EE) and drug loading (DL) were calculated *via* the following equations:

$$\mathrm{EE} = \frac{m_{\mathrm{exp}}}{m_{\mathrm{i}}},$$

$$\mathrm{DL} = \frac{m_{\mathrm{exp}}}{m_{\mathrm{tot}}},$$

where m_{exp} corresponds to the final mass of the encapsulated molecule, m_{i} is the initial mass of the introduced molecule and m_{tot} is the total mass of the copolymer and molecule.

Colloidal stability of *E*/*Z*-micelles. The colloidal stability of the *E*/*Z*-micelles was monitored by DLS. The samples (c = 10 mg mL^{-1} in PBS) were stored at 4 °C, and were sonicated using an ultrasound bath for 10 min prior to each measurement.

Study of the physico-chemical properties

Measurement of the cloud point temperature. The cloud point temperature of the *E*/*Z*-copolymers (c = 1 mg mL^{-1}) was measured by UV-Vis spectroscopy in transmittance mode. Each solution was subjected to heating at 1 °C per 5 min. The transmittance was monitored at λ = 600 nm. The cloud point temperature was determined to be the temperature at which aggregation started, when the transmittance began to decrease.

Aggregation induced emission study. Eleven solutions of either *E*/*Z*-copolymer in a mixture of THF:water at different f_{w} (%) were prepared as follows: 0, 10, 20, 30, 40, 50, 60, 70, 80, 90 and 100%. The concentration of the copolymer (c = 1 mg mL^{-1}) was identical for all solutions. For the solutions with f_{w} ranging from 10% to 90%, a stock solution of copolymer in water, prepared by thin film hydration following the same method used for micelle formulation, was diluted to obtain the desired THF:water volume ratios.

Determination of the relative quantum yield of fluorescence. The relative quantum yields of fluorescence (ϕ_{s}) of both *E*/*Z*-copolymers were determined using the following equation:

$$\varphi_{\mathrm{s}} = \varphi_{\mathrm{r}} \times \frac{A_{\mathrm{r}} I_{\mathrm{s}} n_{\mathrm{r}}^2}{A_{\mathrm{s}} I_{\mathrm{r}} n_{\mathrm{s}}^2},$$

where ϕ_{r} is the fluorescence quantum yield of quinine sulphate in 0.1 M H_2SO_4 (0.54), A is the absorbance intensity at 350 nm, I is the integrated fluorescence intensity (excitation at 350 nm) and n is the refractive index of the media ($n_{\mathrm{r}} = n_{\mathrm{s}} = 1.33$).[53]

Determination of the critical micellar concentration. The CMC was determined by fluorescence using the AIE property of TPE. A stock solution of either *E*/*Z*-copolymer (c = 100 μg mL^{-1}) was diluted to obtain solutions with the following concentrations of copolymer (μg mL^{-1}): 12, 10, 8, 6, 4, 2, 1, 0.5, 0.25, 0.1, 0.05, 0.025, 0.01, 0.005, 0.0025 and 0.001. By plotting the fluorescence intensity at $\lambda \approx 480$ nm against the concentration, two straight lines were obtained. Their intersection was determined to be the CMC value.

In vitro experiments

Cell culture. HeLa cells (human cervical cancer cell line) were routinely maintained in DMEM (Sigma Aldrich) supplemented with 10% (v/v) fetal bovine serum (PAA), penicillin (100 U mL^{-1}, Sigma Aldrich), and streptomycin (100 μg mL^{-1}, Sigma Aldrich).

Cell proliferation/survival assay. HeLa cells suspended in culture medium were seeded at a final density of 1200 cells per well (100 μL per well) into the wells of an optical black-walled, clear-bottom 96-well culture microplate (Costar, #3904) precoated with rat tail collagen (Sigma Aldrich). Plates were then incubated at 37 °C in a humidified incubator with 5% CO_2. After 24 h, cells were treated with micelles at the indicated final concentrations, or with PBS (Sigma Aldrich, #D8662) as the vehicle control. Following a 2 h incubation at 37 °C, the culture supernatant was replaced with 100 μL of fresh medium. For cloud point crossing experiments, cells were immediately heated to 41 °C for 5 min in a preheated ThermoMixer® (Eppendorf) equipped with a plate holder. Plates were then returned to the incubator. 72 h post-micelle treatment, cells were fixed with a 4% (w/v) formaldehyde solution (36% formaldehyde, Sigma Aldrich, #47608) diluted in PBS containing Ca^{2+} and Mg^{2+} (Sigma Aldrich, #D8662) and supplemented with Hoechst 33342 (2 μg mL^{-1} final, Sigma Aldrich, #B2261). Plates were then sealed with aluminum adhesive foil (Corning, #6569) and incubated overnight at 4 °C. The supernatants were subsequently replaced with 200 μL of PBS containing Ca^{2+} and Mg^{2+}, and wells were imaged using a high-content epifluorescence microscope (Operetta, PerkinElmer). Each well was acquired with 9 fields per well at 10× magnification in the blue fluorescence channel (λ_{exc} = 380 ± 20 nm; λ_{em} = 445 ± 35 nm). For image quantification, an automated segmentation and quantification algorithm was developed using Harmony 3.0 software (PerkinElmer). Briefly, the algorithm segmented nuclear regions of interest (ROI) based on Hoechst fluorescence, and quantified the number of cells per field and per well. Results were normalized to vehicle-treated (NT) wells, and expressed as mean ± standard deviation per condition (n = 3).

FRET assay. HeLa cells suspended in culture medium were seeded at a final density of 50 000 cells per well (100 μL per well) into the wells of a 96-well plate V-bottom polystyrene plate (Greiner). Cells were then immediately treated with micelles at the indicated final concentrations, or with PBS as the vehicle control. Following a 2 h incubation at 37 °C, the plate was centrifuged (300 G, 4 min), the supernatants were discarded by aspiration, and the cell pellets were resuspended in 200 μL of PBS. This PBS washing step was repeated twice to remove excess micelles. Cells were finally suspended in 100 μL of PBS, and transferred into the wells of an optical black-walled, clear-bottom 96-well culture microplate (CellVis, #P96-1.5H-N). Cellular fluorescence was acquired with a Clariostar plate reader (BMG Labtech) at the following wavelengths (nm): TPE fluorescence (λ_{exc}: 324–326 nm/λ_{em}: 440–470 nm); DiI fluorescence (λ_{exc}: 528–554 nm/λ_{em}: 604–640 nm); TPE-DiI FRET fluorescence (λ_{exc}: 324–326 nm/λ_{em}: 604–640 nm). Results were

normalized to PBS-treated (NT) wells, and expressed as mean ± standard deviation per condition (n = 3).

Statistics. Statistical data analysis was performed using GraphPad Prism (v9.1.2, GraphPad Software). Student's t-test was used to determine the statistical significance between two groups. The significance of difference was indicated as p (*$p \leq 0.05$, **$p \leq 0.01$, ***$p \leq 0.001$, ****$p \leq 0.0001$) or n.s. (not significant).

Conclusions

This work demonstrates the design and successful synthesis of thermoresponsive copolymer micelles based on poly(2-oxazoline)s with a tetraphenylethylene (TPE) hydrophobic core. By leveraging the stereochemically pure *E* and *Z*-TPE derivatives synthesized *via* the McMurry reaction, we developed triblock copolymers through CROP reactions of 2-oxazolines. These copolymers self-assembled into micelles with remarkable physico-chemical properties, including the efficient encapsulation of hydrophobic molecules. A key outcome of this study is the demonstration of the profound impact of *E*/*Z* stereochemistry on micelle behavior. The separation of both *E*/*Z*-isomers highlighted major differences of the corresponding micelles in colloidal stability, drug encapsulation of hydrophobic molecules, and cellular uptake, ultimately influencing the biological responses. This was evidenced by their distinct cytotoxicity towards HeLa cancer cells and fluorescence imaging capabilities, showing a better selectivity using NBDHEX@*E*-micelles and DiI @*E*-micelles, respectively. Beyond their potential in drug delivery, the *E*-micelles hold great promise for theranostic applications. Owing to their dual fluorescence properties, AIE from TPE and FRET-based emission from fluorescent probes, these micelles enable real-time imaging and tracking. Overall, this work underscores the importance of controlling the stereochemistry of the central unit when designing block copolymers for biomedical applications, paving the way for next-generation multifunctional nanocarriers in therapy and imaging.

Author contributions

S. H.: conceptualization, methodology, formal analysis, funding acquisition, visualization, investigation, writing – original draft, writing – review & editing; G. P.: data curation, investigation, writing; M. V.: data curation, investigation; M. A.: data curation, investigation; C. P.: data curation, investigation, formal analysis; P. S.: data curation, investigation, formal analysis; and O. K.: conceptualization, funding acquisition, project administration, writing – original draft supervision, writing – review & editing.

Conflicts of interest

There are no conflicts to declare.

Data availability

The data supporting this article have been included as part of the ESI.† CCDC 2428365 (E-TPE-2OH) and 2428366 (Z-TPE-2OH) contain the supplementary crystallographic data for this paper.

Acknowledgements

O. Krupka would like to thank the Agence Nationale de la Recherche (ANR) for the Chair Professor Junior support towards the project ANR-22-CPJ1-0026-01 as well as S. H. for the grant awarded within this framework. The authors are thankful to Prof. V. Montembault, Prof. L. Fontaine, A. Benard and K. Zhang for their fruitful discussion and assistance in SEC analysis as well as V. Cougnon for his contribution in synthesizing molecules during his internship.

References

1 (*a*) D. Patel, K. Kuperkar, S. Yusa and P. Bahadur, Nanoscale Self-Assemblies from Amphiphilic Block Copolymers as Proficient Templates in Drug Delivery, *Drugs Drug Candidates*, 2023, **2**(4), 898–922, DOI: **10.3390/ddc2040045**; (*b*) K. Kuperkar, D. Patel, L. I. Atanase and P. Bahadur, Amphiphilic Block Copolymers: Their Structures, and Self-Assembly to Polymeric Micelles and Polymersomes as Drug Delivery Vehicles, *Polymers*, 2022, **14**(21), 4702, DOI: **10.3390/polym14214702**.

2 A. A. D'souza and R. Shegokar, Polyethylene glycol (PEG): a versatile polymer for pharmaceutical applications, *Expert Opin. Drug Delivery*, 2016, **13**(9), 1257–1275, DOI: **10.1080/17425247.2016.1182485**.

3 J. Harris and R. Chess, Effect of pegylation on pharmaceuticals, *Nat. Rev. Drug Discovery*, 2003, **2**, 214–221, DOI: **10.1038/nrd1033**.

4 K. Knop, R. Hoogenboom, D. Fischer and U. S. Schubert, Poly(ethylene glycol) in Drug Delivery: Pros and Cons as Well as Potential Alternatives, *Angew. Chem., Int. Ed.*, 2010, **49**(36), 6288–6308, DOI: **10.1002/anie.200902672**.

5 N. J. Ganson, T. J. Povsic, B. A. Sullenger, J. H. Alexander, S. L. Zelenkofske, J. M. Sailstad, C. P. Rusconi and M. S. Hershfield, Pre-existing anti-polyethylene glycol antibody linked to first-exposure allergic reactions to pegnivacogin, a PEGylated RNA aptamer, *J. Allergy Clin. Immunol.*, 2016, **137**(5), 1610–1613, DOI: **10.1016/j.jaci.2015.10.034**.

6 Y.-C. Hsieh, H.-E. Wang, W.-W. Lin, S. R. Roffler, T.-C. Cheng, Y.-C. Su, J.-J. Li, C.-C. Chen, C.-H. Huang, B.-M. Chen, J.-Y. Wang, T.-L. Cheng and F.-M. Chen, Pre-existing anti-polyethylene glycol antibody reduces the therapeutic efficacy and pharmacokinetics of PEGylated liposomes, *Theranostics*, 2018, **8**(11), 3164–3175, DOI: **10.7150/thno.22164**.

7 A. S. A. Lila, H. Kiwada and T. Ishida, The accelerated blood clearance (ABC) phenomenon: Clinical challenge and

approaches to manage, *J. Control. Release*, 2013, **172**(1), 38–47, DOI: 10.1016/j.jconrel.2013.07.026.

8 M. Bauer, C. Lautenschlaeger, K. Kempe, L. Tauhardt, U. S. Schubert and D. Fischer, Poly(2-ethyl-2-oxazoline) as Alternative for the Stealth Polymer Poly(ethylene glycol): Comparison of in vitro Cytotoxicity and Hemocompatibility, *Macromol. Biosci.*, 2012, **12**(7), 986–998, DOI: 10.1002/mabi.201200017.

9 D. G. van Zyl, L. P. Mendes, R. P. Semper, C. Rueckert and P. Baumhof, Poly(2-methyl-2-oxazoline) as a polyethylene glycol alternative for lipid nanoparticle formulation, *Front. Drug. Delivery*, 2024, **4**, 1383038, DOI: 10.3389/fddev.2024.1383038.

10 M. Dirauf, C. Grune, C. Weber, U. S. Schubert and D. Fischer, Poly(ethylene glycol) or poly(2-ethyl-2-oxazoine) – A systematic comparison of PLGA nanoparticles from the bottom up, *Eur. Polym. J.*, 2020, **134**, 109801, DOI: 10.1016/j.eurpolymj.2020.109801.

11 M. Grube, M. N. Leiske, U. S. Schubert and I. Nischang, POx as an Alternative to PEG? A Hydrodynamic and Light Scaterring Study, *Macromolecules*, 2018, **51**(5), 1905–1916, DOI: 10.1021/acs.macromol.7b02665.

12 T. X. Viegas, M. D. Bentley, J. M. Harris, Z. Fang, K. Yoon, B. Dizman, R. Weimer, A. Mero, G. Pasut and F. M. Veronese, Polyoxazoline: Chemistry, Properties, and Applications in Drug Delivery, *Bioconjugate Chem.*, 2011, **22**(5), 976–986, DOI: 10.1021/bc200049d.

13 R. Hoogenboom, H. M. L. Thijs, M. J. H. C. Jochems, B. M. van Lankvelt, M. W. M. Fijten and U. S. Schubert, Tuning the LCST of poly(2-oxazoline)s by varying composition and molecular weight: alternatives to poly(*N*-isopropylacrylamide)?, *Chem. Commun.*, 2008, 5758–5760, DOI: 10.1039/B813140F.

14 M. Hijazi, M. Schmidt, H. Xia, J. Storkmann, R. Plothe, D. Dos Santos, U. Bednarzick, C. Krumm and J. C. Tiller, Investigations on the thermoresponsive behaviour of copoly(2-oxazoline)s in water, *Polymer*, 2019, **175**, 294–301, DOI: 10.1016/j.polymer.2019.05.040.

15 C. Guerrero-Sanchez, J.-F. Gohy, C. D'Haese, H. Thijs, R. Hoogenboom and U. S. Schubert, Controlled thermoreversible transfer of poly(oxazoline) micelles between an ionic liquid and water, *Chem. Commun.*, 2008, 2753–2755, DOI: 10.1039/B804179B.

16 A. R. Salgarella, A. Zahoranová, P. Šrámková, M. Majerčiková, E. Pavlova, R. Luxenhofer, J. Kronek, I. Lacík and L. Ricotti, Investigation of drug release modulation from poly(2-oxazoline) micelles through ultrasound, *Sci. Rep.*, 2018, **8**, 9893, DOI: 10.1038/s41598-018-28140-3.

17 Z. He, A. Schulz, X. Wan, J. Seitz, H. Bludau, D. Y. Alakhova, D. B. Darr, C. M. Perou, R. Jordan, I. Ojima, A. V. Kabanov and R. Luxenhofer, Poly(2-oxazoline) based micelles with high capacity for 3rd generation taxoids: Preparation, in vitro and in vivo evaluation, *J. Control. Release*, 2015, **208**, 67–75, DOI: 10.1016/j.jconrel.2015.02.024.

18 R. Hoogenboom and H. Schlaad, Thermoresponsive poly(2-oxazoline)s, polypeptoids and polypeptides, *Polym. Chem.*, 2016, **8**(1), 24–40, DOI: 10.1039/C6PY01320A.

19 R. Hoogenboom, M. W. M. Fijten, H. M. L. Thijs, B. M. van Lankvelt and U. S. Schubert, Microwave-assisted synthesis and properties of a series of poly(2-alkyl-2-oxazoline)s, *Des. Monomers Polym.*, 2005, **8**(6), 659–671, DOI: 10.1163/156855505774597704.

20 Z. Varanaraja, N. Hollingsworth, R. Green and C. R. Becer, Poly(2-alkyl-2-oxazoline)-Based Copolymer Library with a Thermoresponsive Behavior in Dodecane, *ACS Appl. Polym. Mater.*, 2023, **5**(7), 5158–5168, DOI: 10.1021/acsapm.3c00625.

21 G. Dellaitre, Telechelic poly(2-oxazoline)s, *Eur. Polym. J.*, 2019, **121**, 109281, DOI: 10.1016/j.eurpolymj.2019.109281.

22 R. Merckx, T. Swift, R. Rees, J. F. R. Van Guyse, E. Schoolaert, K. De Clerck, H. Ottevaere, H. Thienpont, V. V. Jerca and R. Hoogenboom, Förster resonance energy transfer in fluorophore labeled poly(2-ethyl-2-oxazoline)s, *J. Mater. Chem. C*, 2020, **8**(40), 14125–14137, DOI: 10.1039/D0TC02830D.

23 C. Zhu, R. T. K. Kwok, J. W. Y. Lam and B. Z. Tang, Aggregation-Induced Emission: A Trailblazing Journey to the Field of Biomedicine, *ACS Appl. Bio Mater.*, 2018, **1**(6), 1768–1786, DOI: 10.1021/acsabm.8b00600.

24 Y. Xu, G. Li, W. Zhuang, H. Yu, Y. Hu and Y. Wang, Micelles prepared from poly(N-isopropylacrylamide-*co*-tetraphenylethene acrylate)-*b*-poly[oligo(ethane glycol)methacrylate] double hydrophilic block copolymer as hydrophilic drug carrier, *J. Mater. Chem. B*, 2018, **6**(45), 7495–7502, DOI: 10.1039/c8tb02247j.

25 K. Yan, S. Zhang, K. Zhang, Y. Miao, Y. Qiu, P. Zhang, X. Jia and X. Zhao, Enzyme-responsive polymeric micelles with fluorescence fabricated through aggregation-induced copolymer self-assembly for anticancer drug delivery, *Polym. Chem.*, 2020, **11**(48), 7704–7713, DOI: 10.1039/D0PY01328E.

26 L. Yang, S. Fu, L. Liu, Z. Cai, C. Xia, B. Song, Q. Gong, Z. Lu and H. Ai, Tetraphenylethylene-conjugated polycation covered iron oxide nanoparticles for magnetic resonance/optical dual-mode imaging, *Regener. Biomater.*, 2021, **8**(3), rbab023, DOI: 10.1093/rb/rbab023.

27 J.-H. Kim, D. Yim and W.-D. Jang, Thermo-responsive Poly(2-isopropyl-2-oxazoline) and Tetraphenylethene Hybrids for Stimuli-responsive Photoluminescence Control, *Chem. Commun.*, 2016, **55**(22), 4152–4155, DOI: 10.1039/C6CC00722H.

28 H. Wu, L. Zhang, J. Yang, R. Bo, H. Du, K. Lin, D. Zhang, M. Ramachandran, Y. Shen, Y. Xu, X. Xue, Z. Ma, A. R. Lindstrom, R. Carney, T.-Y. Lin and Y. Li, Rotatable Aggregation-Induced-Emission/Aggregation-Caused-Quenching Ratio Strategy for Real-Time Tracking Nanoparticle Dynamics, *Adv. Funct. Mater.*, 2020, **30**(15), 1910348, DOI: 10.1002/adfm.201910348.

29 L. Wu, C. Huang, B. P. Emery, A. C. Sedgwick, S. D. Bull, X.-P. He, H. Tian, J. Yoon, J. L. Sessler and T. D. James, Förster resonance energy transfer (FRET)-based small molecule sensors and imaging agents, *Chem. Soc. Rev.*, 2020, **49**(15), 5110–5139, DOI: 10.1039/C9CS00318E.

30 X. Ma, R. Sun, J. Cheng, J. Liu, F. Gou, H. Xiang and X. Zhou, Fluorescence Aggregation-Caused Quenching versus Aggregation-Induced Emission: A Visual Teaching

Technology for Undergraduate Chemistry Students, *J. Chem. Educ.*, 2016, **93**(2), 345–350, DOI: 10.1021/acs.jchemed.5b00483.

31 J. M. Park, Y. J. Kim and W.-D. Jang, Multimodal Stimuli-Responsive Fluorophore-Functionalized Heterotelechelic Poly(2-isopropyl-2-oxazoline), *ACS Appl. Polym. Mater.*, 2020, **2**(8), 3535–3542, DOI: 10.1021/acsapm.0c00543.

32 B. Kulkarni, S. Qutub, V. Ladelta, N. M. Khashab and N. Hadjichristidis, AIE-Based Fluorescent Triblock Copolymer Micelles for Simultaneous Drug Delivery and Intracellular Imaging, *Biomacromolecules*, 2021, **22**(12), 5243–5255, DOI: 10.1021/acs.biomac.1c01165.

33 Z. Huang, Q. Li, H. Xue, W. Liao, Y. Feng, H. Yuan, L. Tao and Y. Wei, Synthesis of an aggregation-induced emission (AIE) dye with pH-sensitivity based on tetraphenylethylene-pyridine for fluorescent nanoparticles and its applications in bioimaging and in vitro anti-tumor effect, *Colloids Surf. B: Biointerfaces*, 2024, **234**, 113750, DOI: 10.1016/j.colsurfb.2024.113750.

34 N. Yang, Y.-Y. Zhu, W.-X. Lin, Y.-L. Lu and W.-R. Xu, pH-Responsive fluorescent supramolecular nanoparticles based on tetraphenylethylene-labelled chitosan and a six-fold carboxylated tribenzotriquinacene, *Beilstein J. Org. Chem.*, 2023, **19**, 635–645, DOI: 10.3762/bjoc.19.45.

35 Y. Lu, Z. Yue, J. Xie, W. Wang, H. Zhu, E. Zhang and Z. Cao, Micelles with ultralow critical micelle concentration as carriers for drug delivery, *Nat. Biomed. Eng.*, 2018, **2**, 318–325, DOI: 10.1038/s41551-018-0234-x.

36 Y. Jiang and N. Hadjichristidis, Tetraphenylethylene-Functionalized Polyethylene-Based Polymers with Aggregation-Induced Emission, *Macromolecules*, 2019, **52**(5), 1946–1955, DOI: 10.1021/acs.macromol.9b00121.

37 S. Wang, Y. Luo and X. Li, Liquid crystal block copolymer micelles with aggregation-induced emission from corona chains, *J. Phys.: Conf. Ser.*, 2020, **1605**, 012173, DOI: 10.1088/1742-6596/1605/1/012173.

38 L. Mao, S. Dai, M. Zhang, Y. Hou, N. Jiang, X. Gu, Z. Gan and Z. Ning, Effects of tetraphenylethylene groups on the crystallization of poly(L-lactide) with different molecular weights, *Eur. Polym. J.*, 2024, **215**, 113234, DOI: 10.1016/j.eurpolymj.2024.113234.

39 Y. Xie and Z. Li, Recent Advances in the Z/E Isomers of Tetraphenylethene Derivatives: Stereoselective Synthesis, AIE Mechanism, Photophysical Properties, and Application as Chemical Probes, *Chem. – Asian J.*, 2019, **14**(15), 2524–2541, DOI: 10.1002/asia.201900282.

40 (*a*) H. Chen, Y. Fan, X. Yu, V. Semetey, S. Trépout and M.-H. Li, Light-Gated Nano-Porous Capsules from Stereoisomer-Directed Self-Assemblies, *ACS Nano*, 2021, **15**(1), 884–893, DOI: 10.1021/acsnano.0c07400; (*b*) H. Chen, X. Yu, Y. Fan, S. Trépout and M.-H. Li, Nanoporous Vesicular Membranes of Amphiphilic Polymers Containing Trans/Cis Isomers, *CCS Chem.*, 2022, **4**(8), 2651–2661, DOI: 10.31635/ccschem.022.202201916.

41 Z. Lu, S. Yang, X. Liu, Y. Qin, S. Lu, Y. Liu, R. Zhao, L. Zheng and H. Zhang, Facile synthesis and separation of *E*/*Z* isomers of aromatic-substituted tetraphenylethylene for investigating their fluorescent properties via single crystal analysis, *J. Mater. Chem. C*, 2019, **7**(14), 4155–4163, DOI: 10.1039/C9TC00446G.

42 W. C. Griffin, Classification of Surface-Active Agents by "HLB", *J. Cosmet. Sci.*, 1949, **1**(5), 311–326.

43 M. Glassner, D. R. D'hooge, J. Y. Park, P. H. M. Van Steenberge, B. D. Monnery, M.-F. Reyniers and R. Hoogenboom, Systematic investigation of alkyl sulfonate initiators for the cationic ring-opening polymerization of 2-oxazoline revealing optimal combinations of monomers and initiators, *Eur. Polym. J.*, 2015, **65**, 298–304, DOI: 10.1016/j.eurpolymj.2015.01.019.

44 X. Fang, Y.-M. Zhang, K. Chang, Z. Liu, X. Su, H. Chen, S. X.-A. Zhang, Y. Liu and C. Wu, Facile Synthesis, Macroscopic Separation, E/Z Isomerization, and Distinct AIE properties of Pure Stereoisomers of an Oxetane-Substituted Tetraphenylethene Luminogen, *Chem. Mater.*, 2016, **28**(18), 6628–6636, DOI: 10.1021/acs.chemmater.6b02746.

45 J. Wang, Q. Jiang, S. Cao, C. Sun, Y. Zhang, Y. Qiu, H. Wang, G. Yin, Y. Liao and X. Xie, Z/E Effect on Phase Bhevaior of Main-Chain Liquid Crystalline Polymers Bearing AIEgens, *Macromolecules*, 2021, **54**(23), 10740–10749, DOI: 10.1021/acs.macromol.1c02051.

46 W. J. Leigh and D. R. Arnold, Merostabilization in radical ions, triplets, and biradicals. 5. The thermal cis–trans isomerization of para-substituted tetraphenylethylenes, *Can. J. Chem.*, 1981, **59**(3), 609–620, DOI: 10.1139/v81-089.

47 (*a*) F. Wiesbrock, R. Hoogenboom, C. H. Abeln and U. S. Schubert, Single-Mode Microwave Ovens as New reaction Devices: Accelerating the Living Polymerization of 2-Ethyl-2-Oxazoline, *Macromol. Rapid Commun.*, 2004, **25**(22), 1895–1899, DOI: 10.1002/marc.200400369; (*b*) K. P. Luef, R. Hoogenboom, U. S. Schubert and F. Wiesbrock, Microwave-assisted cationic ring-opening polymerization of 2-oxazolines, *Adv. Polym. Sci.*, 2015, **274**, 183–208, DOI: 10.1007/12_2015_340.

48 W. Zhao, Z. Li, N. Liang, J. Liu, P. Yan and S. Sun, AIE-Featured Redox-Sensitive Micelles for Bioimaging and Efficient Anticancer Drug Delivery, *Int. J. Mol. Sci.*, 2022, **23**(18), 10801, DOI: 10.3390/ijms231810801.

49 J. Wang, J. Mei, R. Hu, J. Z. Sun, A. Qin and B. Z. Tang, Click Synthesis, Aggregation-Induced Emission, E/Z Isomerization, Self-Organization, and Multiple Chromisms of Pure Stereoisomers of a Tetraphenylethene-Cored Luminogen, *J. Am. Chem. Soc.*, 2012, **134**(24), 9956–9966, DOI: 10.1021/ja208883h.

50 H. Sha, S. Dong, C. Yu, R. Zou, Y. Zhu, Y. Lu, J. Zhang, H. Cao, D. Chen, J. Wu and J. Feng, In Vitro and in Vivo Efficacy of NBDHEX on Gefitinib-resistant Human Non-small Cell Lung Cancer, *J. Cancer*, 2020, **11**(24), 7216–7223, DOI: 10.7150/jca.46461.

51 J. Lim, M. Petersen, M. Bunz, C. Simon and M. Schindler, Flow cytometry based-FRET: basics novel, developments and future perspectives, *Cell. Mol. Life Sci.*, 2022, **79**(4), 217, DOI: 10.1007/s00018-022-04232-2.

52 J. Sikkema, J. A. de Bont and B. Poolman, Mechanisms of membrane toxicity of hydrocarbons, *Microbiol. Rev.*, 1995, **59**(2), 201–222, DOI: **10.1128/mr.59.2.201-222.1995**.

53 A. Barras, F. Sauvage, I. de Hoon, K. Braeckmans, D. Hua, G. Buvat, J. C. Faire, C. Lethien, J. Sebag, M. Harrington, A. Abderrahmani, R. Boukherroub, S. De Smedt and S. Szunerits, Carbon quantum dots as a dual platform for the inhibition and light-based destruction of collagen fibers: implications for the treatment of eye floaters, *Nanoscale Horiz.*, 2021, **6**, 449–461, DOI: **10.1039/D1NH00157D**.